SLAC–PUB–5585
CU-TP-524
June 1991
T/E

NEW QCD PRODUCTION MECHANISMS FOR HARD PROCESSES AT LARGE $x^{\star}$

STANLEY J. BRODSKY AND PAUL HOYER[†]

Stanford Linear Accelerator Center

Stanford University, Stanford, California 94309

and

A. H. MUELLER[‡] AND WAI-KEUNG TANG[‡]

Department of Physics

Columbia University, New York, NY 10027

Submitted to *Nuclear Physics B*

⋆ Work supported in part by the Department of Energy, contract DE-AC03-75SF00525.
† Permanent address: Department of High Energy Physics, University of Helsinki, Finland. Work supported by the Academy of Finland.
‡ Supported in part by the Department of Energy

ABSTRACT

We study the QCD production mechanisms for lepton and quark pairs of high mass $\mathcal{M}$ that carry a large fraction x of the projectile momentum. We show that the dominant contribution comes from peripheral processes in which low x spectator quarks interact with the target, with the hardness scale of the collision being given by $Q^2 = \mathcal{M}^2(1-x)$. In the high $\mathcal{M}^2$ limit with fixed $\mathcal{M}^2(1-x)$ we identify new leading-order perturbative contributions from the hadron wavefunction which involve more than one constituent. These 'intrinsic' contributions cannot be expressed in terms of the usual single-parton structure functions, implying a breakdown of QCD factorization. In a numerical study of a simple gauge theory model, we show that such contributions can dominate the standard single-parton factorizable terms. These results appear to explain several anomalies seen in the data: the excess production and the anomalous nuclear-number dependence of open and bound charm at large x; the 'cumulative' effects ($x > 1$) observed in hadron production from nuclei; and the large target polarization asymmetry observed for hadron production at high x. The intrinsic multi-parton processes provide new mechanisms for the hadro-production of the J/ψ directly in a color-singlet state and also for the production of heavy flavor systems in lepto-production at high momentum.

1. Introduction

The data[1,2,3] on high momentum J/ψ production in hadron-nucleus collisions exhibit a surprising result. When the nuclear number (A) dependence of the J/ψ production cross section is parametrized as A^α, the effective power α decreases with the fractional momentum x of the J/ψ. Data at different energies show that indeed $\alpha = \alpha(x)$, *i.e.* the nuclear suppression obeys Feynman scaling.[4] In particular, the power α is not a function of x_2, the fraction of momentum taken from the nucleus and given to the J/ψ. This result violates the perturbative QCD factorization prediction for hard processes, and thus its explanation must lie in higher twist effects.

A phenomenological interpretation of the J/ψ A-dependence was given in Ref. 5. It was suggested that at large x $c\bar{c}$ production is dominated by an intrinsic component,[6] a component whose probability in the infinite momentum wavefunction of the hadron scales as an inverse power of M_c^2, and that the $c\bar{c}$ is 'freed' from its virtual state by interactions of the light quarks in the projectile hadron with the target nucleus. Because the interaction of the light quark components with nucleons is expected to be strong, one should then expect that nuclear cross sections will be surface dominated, *i.e.* $\alpha \simeq 2/3$. This nuclear suppression is unrelated to the shadowing of parton distributions seen in deep inelastic scattering. At first sight this proposal seems to contradict the usual understanding[7] that it requires a hard scattering to 'free' a heavy quark pair from its virtual state and allow it to be produced. It is the main purpose of this paper to reconcile the picture of Ref. 5 with calculations of hard processes in QCD, and to exhibit how this works in detail for heavy quark production in an Abelian model with scalar quarks.

In deriving the QCD predictions for large x massive pairs we must distinguish

between the three limits

$$\mathcal{M} \to \infty,\ x \to 1 \ \text{ with } \ \mathcal{M}^2(1-x) \to \infty, \tag{1.1}$$

$$\mathcal{M} \to \infty,\ x \to 1 \ \text{ with } \ \mathcal{M}^2(1-x) \ \text{ fixed}, \tag{1.2}$$

$$\mathcal{M} \to \infty,\ x \to 1 \ \text{ with } \ \mathcal{M}^2(1-x) \to 0. \tag{1.3}$$

In the first limit (1.1) the usual perturbative QCD scattering formalism applies, including the factorization theorem for hard subprocesses.[8] The effective scale of the interaction, $\mathcal{M}^2(1-x)$, is still asymptotically large. Intrinsic higher twist diagrams, in which the pair is coupled to more than one constituent of the projectile, are damped by powers of $\mathcal{M}^2(1-x)$. In the last limit (1.3), the standard spectator counting rules for the power behavior of structure functions in the $x \to 1$ limit become valid.[9,10]

It is quite interesting to consider the behavior of the QCD processes in the intermediate case of the limit (1.2), in which $\mathcal{M}^2(1-x)$ is held fixed. It turns out that subprocesses involving spectator constituents, which would give power–suppressed higher twist contributions in the limit (1.1), contribute at leading order in the limit (1.2). Hence the distinction between 'extrinsic' processes, where the pair is created by a single gluon, and 'intrinsic' processes, where the pair is created by several gluons, essentially disappears. An immediate consequence of the fact that several partons are involved in the leading subprocesses is that the QCD factorization theorem breaks down: Scattering cross sections can no longer be expressed in terms of single parton distributions of the colliding hadrons. We believe that these observations can provide a framework for understanding several

puzzling phenomena observed at large x, and in particular for explaining the A-dependence of J/ψ production.

We find that one can indeed free a virtual $c\bar{c}$ pair, or a lepton pair, at large x by a relatively soft interaction with a light quark component of the projectile. The hardness of the interaction has scale $\mathcal{M}^2(1-x)$, where $\mathcal{M}$ is the pair mass, and the 'freeing' probability is proportional to $1/\mathcal{M}^2(1-x)$. Thus, at sufficiently large x, the cross section for freeing the pair will become large enough so that an x-dependent departure from an A^1 dependence can be expected in the nuclear cross section. If the reaction freeing the pair occurs for an extrinsic, leading-twist component of the projectile, a component of the infinite momentum wavefunction scaling logarithmically with $\mathcal{M}^2$, then the resulting cross section in the limit (1.1) is just the normal factorized expression for $q\bar{q}$ annihilation in perturbative QCD. If the freeing occurs for an intrinsic component it corresponds to a higher twist effect in the usual hard scattering formalism.

In Section 2 we begin by studying muon pair production in electron-electron collisions in QED. We show that at large x,

$$\mathcal{M}^2 \frac{d\sigma}{d\mathcal{M}^2 dx} \propto \frac{1}{\mathcal{M}^2(1-x)} \tag{1.4}$$

and that the factor $1/\mathcal{M}^2(1-x)$ can be interpreted as the probability of the muon pair being freed from the electron. The freeing becomes easier at large x because the coherence of the incoming electron-muon-pair Fock state is easily broken by deflecting the electron, which carries a small fraction of the incident momentum, as the system passes the target electron. We also observe that the usually dominant $\gamma\gamma$ fusion mechanism is relatively ineffective at large x because the interaction of the target with the muon pair dipole moment is much weaker than with the

companion electron. The cross section from $\gamma\gamma$ fusion scales as $1/\mathcal{M}^2$ rather than as $1/\mathcal{M}^2(1-x)$. We then discuss how these QED calculations generalize to the situation of large mass lepton and quark pair production in hadron scattering in the limit (1.1), where the usual hard scattering formalism can be applied.

In Section 3 we study the modifications to the standard QCD formalism in the limit (1.2), where $\mathcal{M}^2(1-x)$ is held fixed. The crucial observation is that the high x, high mass pair is created from a Fock state of the projectile whose overall transverse cross section is small, of order $(1-x)/m_h^2$, where m_h is a typical hadronic scale, $m_h \sim 1/\text{fm}$. The lifetime τ of such Fock states is short,

$$\tau \sim (1-x)p/m_h^2 \sim p/\mathcal{M}^2, \tag{1.5}$$

where p is the momentum of the projectile. As this is similar to the lifetime of the high mass pair itself, the virtual pair can be created with no extra power suppression in the asymptotically large variables. In fact, the pair creation probability is determined by the fixed product $\mathcal{M}^2(1-x)$. Moreover, the proximity in transverse space of all Fock state constituents allow them to interact during the lifetime of the virtual pair. Hence leading–twist subprocesses do not dominate[11] in the limit (1.2), and QCD factorization breaks down. In Subsections 3.2 - 3.3 we verify our conclusions by explicit calculations in an abelian model with scalar quarks. In this model, the intrinsic (non-factorizable, multi-parton) contributions to the pair production cross section and structure function turn out to dominate the extrinsic contributions for moderate values of $\mathcal{M}^2(1-x)$.

Section 4 contains a discussion of the implications of our results for a number of observed phenomena at high x, as well as suggestions for future experimental and

theoretical work. Some useful formulas relating hadronic gluon source amplitudes to the gluon structure function are given in the Appendix.

2. Fermion Pair Production at Leading Twist

In this Section we wish to study the production of a lepton or quark pair of large mass $\mathcal{M}$ and high fractional momentum x in the scattering of a single incoming lepton or quark at high energy. We first consider the pure QED process $e^+e^- \to \mu^+\mu^- + e^+e^-$, and then discuss how our result is reconciled with the standard QCD formalism for hard hadron collisions in the limit (1.1).

2.1 Muon Pair Production in Electron-Electron Collisions

We shall study the process $e(p)\,e(P) \to \mu^+\mu^- + e(p')\,e(P')$, where $e(p)$ refers to an incident (massless) electron of momentum p. We use the notation $p^\mu = (p^-, p^+, \vec{p}_\perp)$, where $p^\pm = (p^0 \pm p^3)/\sqrt{2}$. We will be particularly interested in the region $p'^+/p^+ = 1-x \ll 1$, where $p^\mu = (0, p^+, \vec{0}_\perp)$ and $p'^\mu = (p'^2_\perp/2p'^+, p'^+, \vec{p}'_\perp)$. We suppose the pair production takes place in a high energy scattering of the initial electron off a target electron of momentum P.

It is instructive to compare the $\gamma\gamma$ fusion graph illustrated in Fig. 1 with those illustrated in Fig. 2, where the muon pair is only indirectly connected to the target electron, P. The production cross-section is given as the discontinuity, in $s = (p+P)^2$, of the forward elastic electron-electron scattering amplitude. In what follows we shall use the definitions of the target source terms and structure functions given in the Appendix, where now A_μ refers to the abelian electromagnetic field and G refers to the photon distribution in an electron.

The production mechanism illustrated in Fig. 1 is the traditional $\gamma\gamma$ fusion mechanism, and one may immediately write

$$\frac{d\sigma}{d\mathcal{M}^2} = \int_0^1 dx_1 dx_2\, \delta(x_1 x_2 s - \mathcal{M}^2)\, \hat{\sigma}_{\gamma\gamma}(\mathcal{M}^2)\, G(x_1, \mathcal{M}^2)\, G(x_2, \mathcal{M}^2) \tag{2.1}$$

where $\mathcal{M}$ is the mass of the muon pair, $\hat{\sigma}_{\gamma\gamma}$ is the cross section for $\gamma\gamma \to \mu^+\mu^-$ and $G(x, \mathcal{M}^2)$ is the order α contribution of the photon distribution in an electron. The longitudinal momentum fractions of p and P carried by k_1 and k_2 are denoted by x_1 and x_2, respectively. Our interest here is in large x muon pair production, with x the fraction of the longitudinal momentum of p carried by the pair. Thus $x \simeq x_1$ and

$$\mathcal{M}^2 x\, \frac{d\sigma}{d\mathcal{M}^2 dx} = \hat{\sigma}_{\gamma\gamma}(\mathcal{M}^2)\, x G(x, \mathcal{M}^2)\, x_2 G(x_2, \mathcal{M}^2) \tag{2.2}$$

where $x x_2 s = \mathcal{M}^2$. Since $x_2 G(x_2, \mathcal{M}^2) \sim$ constant as $x_2 \to 0$, the cross section given in Eq. (2.2) behaves as $1/\mathcal{M}^2$ at high energy and at large x. The $1/\mathcal{M}^2$ behavior has a simple physical interpretation. In the target rest frame and for large p^+ the projectile electron can have a $\mu^+\mu^-$ component in its wavefunction. The probability of this muon pair component is only logarithmically dependent on the muon pair mass. The μ^+ and μ^- in the pair have a transverse separation of order $1/\mathcal{M}$ and hence form a compact, electrically neutral system. When passing the target, the amplitude for 'freeing' the muon pair from the incoming electron is proportional to the dipole moment of the pair, that is, proportional to $1/\mathcal{M}$. Thus the cross section for freeing the pair is of order $1/\mathcal{M}^2$, as given in Eq. (2.2).

Now consider the contributions illustrated in Fig. 2, in which the target photon interacts directly with the incoming electron. The contribution of the first of the

graphs shown in Fig. 2 is, in terms of the photon source amplitude $\mathcal{S}_{\mu\nu}$ defined in the Appendix,

$$\sigma = \frac{e^6}{2s}\int \frac{d^2\vec{\ell}_\perp\, d\ell^-}{(2\pi)^3}\,\mathcal{S}_{\mu\nu}(\ell)\,\frac{d^4k}{(2\pi)^4k^2}\,2\pi\delta[(p-k+\ell)^2]\,Im\,\Pi(k^2)\,\frac{g_{\alpha\beta}\mathrm{tr}^{\alpha\beta,\mu\nu}}{[(p-k)^2]^2} \quad (2.3)$$

where

$$Im\,\Pi(k^2) = \frac{1}{12\pi}\left(1-\frac{4m_\mu^2}{k^2}\right)^{1/2}\left(1+\frac{2m_\mu^2}{k^2}\right)\Theta(k^2-4m_\mu^2) \quad (2.4)$$

and

$$\mathrm{tr}^{\alpha\beta,\mu\nu} = \mathrm{tr}\{\gamma\cdot p\gamma^\alpha\gamma\cdot(p-k)\gamma^\nu\gamma\cdot(p-k+\ell)\gamma^\mu\gamma\cdot(p-k)\gamma^\beta\}\,. \quad (2.5)$$

We have used current conservation to replace $(g_{\alpha\beta}k^2-k_\alpha k_\beta)\Pi(k^2)$ by $k^2g_{\alpha\beta}\Pi(k^2)$. In a covariant gauge calculation we may replace $\mathcal{S}_{\mu\nu}\mathrm{tr}_\alpha{}^{\alpha,\mu\nu}$ by $\mathcal{S}^{--}\mathrm{tr}_\alpha{}^{\alpha,++}$. Including all four graphs shown, or implied, in Fig. 2 and writing $d^4k = (dk^+/2k^+)dk^2d^2\vec{k}_\perp$ we find for the pair production cross section

$$\sigma = \frac{\alpha^3}{sp^+}\int\frac{d^2\vec{\ell}_\perp}{(2\pi)^3}\mathcal{S}^{--}\,\frac{d\mathcal{M}^2}{\mathcal{M}^2}\,\frac{dx}{x(1-x)}\,d^2\vec{k}_\perp\,Im\,\Pi(\mathcal{M}^2)\,\frac{\mathrm{Tr}^{++}}{\mathrm{Den}} \quad (2.6)$$

where $x = k^+/p^+$ and $k^2 = \mathcal{M}^2$. In the $x\to 1$ limit we get

$$\frac{\mathrm{Tr}^{++}}{\mathrm{Den}} \approx -16{p^+}^2(1-x)\left[\frac{\vec{k}_\perp}{k_\perp^2+\mathcal{M}^2(1-x)} - \frac{\vec{k}_\perp-\vec{\ell}_\perp}{(\vec{k}_\perp-\vec{\ell}_\perp)^2+\mathcal{M}^2(1-x)}\right]^2\,. \quad (2.7)$$

The leading contribution in the $\vec{k}_\perp$ integration of (2.6) comes from the region $k_\perp^2 \propto \mathcal{M}^2(1-x)$. Similarly, to pick up the leading logarithm in $\mathcal{M}^2(1-x)$ from

the $\vec{\ell}_\perp$ integral, the relevant region is $\ell_\perp^2 \ll \mathcal{M}^2(1-x)$. In this region

$$\frac{\mathrm{Tr}^{++}}{\mathrm{Den}} \approx -\frac{16{p^+}^2(1-x)}{[\mathcal{M}^2(1-x)+k_\perp^2]^2}\left[\vec{\ell}_\perp - \frac{2\vec{k}_\perp\,\vec{k}_\perp\cdot\vec{\ell}_\perp}{\mathcal{M}^2(1-x)+k_\perp^2}\right]^2 . \tag{2.8}$$

Averaging over the angle between $\vec{k}_\perp$ and $\vec{\ell}_\perp$ gives

$$\left\langle\frac{\mathrm{Tr}^{++}}{\mathrm{Den}}\right\rangle \approx -\frac{16{p^+}^2\ell_\perp^2}{[\mathcal{M}^2(1-x)+k_\perp^2]^2}\left\{1-\frac{2k_\perp^2\mathcal{M}^2(1-x)}{[\mathcal{M}^2(1-x)+k_\perp^2]^2}\right\} . \tag{2.9}$$

Substituting Eq. (2.9) in (2.6) one finds

$$\mathcal{M}^2\frac{d\sigma}{d\mathcal{M}^2dx} \approx \frac{16\pi}{3}\,Im\,\Pi(\mathcal{M}^2)\,\frac{\alpha^3}{\mathcal{M}^2(1-x)}\,x_2G(x_2,\mathcal{M}^2(1-x)) \tag{2.10}$$

with $x_2 = \mathcal{M}^2/s$ as in Eq. (2.2).

Note that in contrast to Eq. (2.2), the cross section in (2.10) behaves as $1/\mathcal{M}^2(1-x)$ and thus this contribution dominates $\gamma\gamma$ fusion by a power of $1/(1-x)$ when $1-x$ is small. This fact can also be readily understood on physical grounds. Recall that we have interpreted the $1/\mathcal{M}^2$ behavior of the right hand side of Eq. (2.2) as the square of the dipole moment of the $\mu^+\mu^-$ pair when it occurs as a virtual fluctuation in the wavefunction of a fast electron. Now suppose that a fast electron, p, passes a stationary target, P. The fast electron may consist of a single bare electron, or it may consist of a bare electron and a virtual photon, or it may consist of a bare electron and a virtual $\mu^+\mu^-$ pair. If these three components react differently as the system passes the target, the coherence between the components is lost, and either photon or muon pair production may occur. The muon pair has a small dipole moment, and so it interacts very weakly with the target electron. However, if the muon pair carries almost all of the momentum of the incoming

state its companion electron, with $p' = (p - k)$ in Fig. 2, has a small longitudinal momentum and thus is rather easy to deflect. A significant deflection will break the coherence of the system and free the μ-pair. The angular deflection is proportional to $\Delta(p-k)_\perp/(p-k)^+ = \ell_\perp/(p-k)^+$, which is proportional to $1/(1-x)$. Thus we can understand the additional $1/(1-x)$ factor as expressing the relative ease with which the coherence of the incoming state is broken when one deflects the companion electron to the muon pair. This is in agreement with the claim made in Ref. 5. This fact is perhaps surprising since normally one expects that it requires a hard scattering to free a heavy particle.[7] Here we see that the $x \to 1$ region is special, and that a heavy particle, or a heavy particle pair, can be freed by a relatively soft interaction in the restricted, $x \to 1$ region of phase space.

2.2 Pair Production in Hadron Collisions

Now let us come back to QCD and consider both lepton and heavy quark pair production in hadron collisions. For lepton pair production at large x in a quark-hadron collision, the factorized formula (2.10) remains valid after a replacement of one of the α's in Eq. (2.10) by $\alpha_s/2N_c$ while the remaining α^2 stays as α^2_{QED}. But the discussion leading up to Eq. (2.10) and the dominance of the diagram in Fig. 2 do not seem to fit in with the usual hard scattering QCD formalism in which lepton pair production is viewed as quark-anti-quark annihilation into a virtual photon. In order to make contact with the normal QCD Drell–Yan mechanism we must consider hadron-hadron scattering. In Fig. 3 we show the diagram analogous to the first diagram of Fig. 2.

Now since the lepton pair should carry most of the hadron momentum, this must also be true of the quark line p in Fig. 3, from which the pair is radiated. As

we shall show in the next section, this implies that the quark line p has a virtuality of order $m_h^2/(1-x)$, where m_h is a typical hadronic scale. The factorization of the lepton pair creation subprocess is possible only if the hardness $\mathcal{M}^2$ of the pair is bigger than the virtuality of the quark line p. Thus we must require that $m_h^2/(1-x) \ll \mathcal{M}^2$, so that effectively we are dealing with the limit (1.1). We shall return to the situation that pertains in limit (1.2) in Section 3.

Let us then consider the contribution of the diagram in Fig. 3 to lepton pair production in the limit (1.1). If we substitute Eq. (2.10) inside the graph shown in Fig. 3 we encounter a singular integral. To see what happens, call $y = k^+/p^+$ and $x = k^+/p_h^+$. In Fig. 3 we must integrate y between x and 1. However, the $1/(1-x)$ factor is replaced by $1/(1-y)$ and the dy integration is singular. Since $k_\perp^2 \propto \mathcal{M}^2(1-y)$ we may interpret the $dy/(1-y)$ integral as $dk_\perp^2/k_\perp^2$; the divergence we are faced with is thus nothing other than the usual logarithmic $k_\perp$ integral over the virtuality of the line $p-k$. This is the signal that we should factorize the leading order in α_s contribution of Fig. 3 as

$$\mathcal{M}^2 \frac{d\sigma}{d\mathcal{M}^2 dx} = q(x, \mathcal{M}^2(1-x))\, \widehat{\sigma}_{q\bar{q}}(\mathcal{M}^2) \bar{q}(x_2, \mathcal{M}^2(1-x)) \qquad (2.11)$$

with $\widehat{\sigma}_{q\bar{q}}$ the $q\bar{q} \to \mu^+\mu^-$ cross section, $\widehat{\sigma}_{q\bar{q}}(\mathcal{M}^2) \sim 1/\mathcal{M}^2$. Thus we recover, in the limit (1.1), the usual Drell-Yan expression for lepton pair production in QCD, but with the structure functions evaluated at the relatively soft scale $\mathcal{M}^2(1-x)$.

Let us now apply the same procedure to heavy quark pair production in hadron collisions, at large x-values in the limit (1.1). Traditional QCD hard scattering arguments tell us that the heavy quark pair, $c\bar{c}$, can be produced in two ways: (i) $gg \to c\bar{c}$, and (ii) $q\bar{q} \to c\bar{c}$. The discussion which we have given for QED in the last section suggests that the $q\bar{q}$ mechanism should dominate by a full power

of $1/(1-x)$. This is indeed the case, since the ratio of gluon to quark structure functions satisfies

$$\frac{G(x, \mathcal{M}^2(1-x))}{q(x, \mathcal{M}^2(1-x))} \propto 1-x \tag{2.12}$$

when $1-x$ is small. Thus we see that large x heavy quark production is dominated by the $q\bar{q} \to c\bar{c}$ subprocess and obeys Eq. (2.11) but with $\widehat{\sigma}_{q\bar{q}}$ now referring to the $q\bar{q} \to c\bar{c}$ cross section. Our physical interpretation given for muon pair production in electron-electron scattering also applies to heavy quark production in QCD. As a fast incoming hadron passes the target, the virtual $c\bar{c}$ pair is mostly freed not by a direct interaction between the c or $\bar{c}$ and the target, but rather by the interaction of a light quark in the projectile, which frees the $c\bar{c}$ pair by breaking the coherence of the $c\bar{c}$ in the hadron's wavefunction.

This interpretation may seem rather curious given that the $c\bar{c}$ pair is in an octet state and interacts strongly with the target hadron, in contrast to the weak dipole interaction of the $\mu^+\mu^-$ pair we discussed in QED. Indeed the $c\bar{c}$ pair does interact strongly with the target hadron. However, the interaction with the total charge of the $c\bar{c}$ pair does not differ from the interaction with the gluon which produced it; hence the coherence of the g and $c\bar{c}$ components in the wavefunction of the hadron is not broken. The color dipole of the $c\bar{c}$ does distinguish the pair from a gluon and so this (weak) dipole interaction can free the $c\bar{c}$ exactly as for the $\mu^+\mu^-$ in electrodynamics.

3. Factorization–Breaking in a New QCD Limit

3.1 Scaling Behavior at Large x

Let us consider, for a moment, the physics of the $x \to 1$ end-point behavior of structure functions. For the following discussion we may assume $\mathcal{M}$ to be fixed, or we may take the limit (1.3), in which $\mathcal{M} \to \infty$ but $\mathcal{M}^2(1-x) \to 0$. The essential behavior of hadronic structure functions in QCD is then controlled by power laws $(1-x)^n$, where n is determined by the number of constituents in the hadron.[9] The conceptual picture for this behavior is quite simple. Kinematically, a Fock state where one constituent carries most of the momentum must be far off-shell, and thus it has a brief life-time. In time-ordered perturbation theory, the energy deficiency of a Fock state is given by

$$\Delta E = \frac{1}{2p}\left(M^2 - \sum_i \frac{m_i^2 + k_{i\perp}^2}{x_i}\right) \tag{3.1}$$

when the total momentum p of the hadron is large (or, more generally, for arbitrary light-cone momentum p^+). Here M is the hadron rest mass and the sum is over all partons. Recalling that $\sum x_i = 1$ due to momentum conservation, the limit $x \to 1$ for one parton forces all the other x_i's to vanish, leading to a large energy difference (3.1). Hence, by the uncertainty principle, the life-time of the state is proportional to $1-x$. Thus for $x \to 1$ the behavior of the Fock state amplitude can be calculated as a perturbation on the long-lived, non-perturbative wavefunction.

A typical Feynman diagram that allows the transfer of almost all the momentum in a proton wavefunction to one parton is shown in Fig. 4. Notice that all the constituents in the valence Fock state have to be involved, as each carries a finite momentum fraction in the non-perturbative wavefunction. Moreover, the entire

momentum transfer must take place within a time-scale comparable to the Fock state life-time $\sim (1-x)p/m_h^2$, where $m_h \simeq 300$ MeV is a hadronic mass scale. But this is only possible provided that the transverse separations of all constituents vanish in the limit $x \to 1$. The dependence of the mean transverse distance scale $r_\perp$ on $1-x$ can be seen by noting that since the virtuality of the intermediate states in the proton structure function of Fig. 4 are of order $m_h^2/(1-x)$; this is also the effective upper limit of the square of the transverse momenta $k_{i\perp}^2$ of the valence quarks in the proton. Hence only wavefunction components having $r_\perp^2 \approx \mathcal{O}((1-x)/m_h^2)$ contribute as $x \to 1$.

The origin of the spectator counting rules[9] for the power-law dependence of structure functions at $x \to 1$ is thus clear. Each of the internal propagators in Fig. 4 has a virtuality of $\mathcal{O}(m_h^2/(1-x))$. Simple power counting, completely analogous to that done for exclusive form factors,[10] then gives a behavior for the structure function $F(x)$ of the form

$$F(x) \propto (1-x)^{2n_s-1} \tag{3.2}$$

where n_s is the number of partons whose momenta vanish in the $x \to 1$ limit.[12] The constant of proportionality in Eq. (3.2) can be obtained from the distribution amplitude, *i.e.* from the wavefunction evaluated at zero transverse distance between all constituents.

The above picture of multiply–connected transversely–compact Fock states giving rise to the leading $x \to 1$ behavior of structure functions may be compared with the situation for typical single parton hard QCD processes at fixed $x < 1$, such as massive pair production. Figure 5a shows a leading-twist contribution to the production of a fermion pair of high mass $\mathcal{M}$ in a peripheral interaction of a meson

with a target. We take the center of mass energy to be much larger than $\mathcal{M}$, and the momentum exchange ℓ to the target to be small (and mainly transverse). The (proper) lifetime of the intermediate state indicated by the vertical line in Fig. 5a is short, of order $1/\mathcal{M}$, whereafter it decays by emitting the pair. A representative multi-parton contribution to the same process is shown in Fig. 5b.[13] For this diagram to influence the hard process, the time-scale of the interaction with the spectator constituent must be similarly short. Hence the transverse separation of the valence quarks in the meson can be at most $1/\mathcal{M}$. The probability for this is proportional to the transverse area, $1/\mathcal{M}^2$, which explains the power-law suppression of such higher-twist contributions to hard processes.

However, in the combined $x \to 1$, large $\mathcal{M}$ limit (1.2), where $\mathcal{M}^2(1-x)$ is held fixed, the power-counting for multi-parton processes works differently. As argued above, the transverse separation of the two quarks behaves as $\sqrt{1-x}/m_h \sim 1/\mathcal{M}$. Hence in this limit the diagram of Fig. 5b is not in fact suppressed compared to that of Fig. 5a, since the quarks are close enough for them to interact within the time-scale of the hard process. Actually, since the non-perturbative wavefunction is damped as $x \to 1$, the diagram 5a does not contribute significantly in the combined limit (1.2). Thus the leading QCD contribution in this limit arises from multi-parton diagrams such as Fig. 5b, which gives an 'extrinsic' leading order QCD contribution to massive pair production at high x.

It is important to note that in the combined limit (1.2) there are also other types of multi-parton diagrams, in addition to the extrinsic ones, which contribute at leading order in PQCD. One such contribution, which involves both constituents of the non-perturbative meson wavefunction, is shown in Fig. 5c. This is the QCD manifestation of 'Intrinsic Heavy Flavor', previously suggested[6] (on phenomeno-

logical grounds) to be significant for charm production at large x. As we shall see below, these intrinsic diagrams can numerically dominate the extrinsic contributions in the limit (1.2), and lead to qualitatively new physical effects.

Since both extrinsic and intrinsic processes require point-like configurations of the beam hadron as $x \to 1$, one might expect an A^1 behavior for nuclear cross sections. For example, in Fig. 5b the transverse separation of the valence quarks is of order $r_\perp \sim \sqrt{1-x}/m_h$ at the time of exchange of the virtual gluon j. Nevertheless, the transverse velocities of the 'stopped' lines p_1 and p_2 are large because of their small longitudinal momenta. From the results of Section 2, or directly from the expression (3.1), it can be seen that the transverse momenta of those lines are given by the hardness scale of the interaction, $p_{1\perp}^2 \sim p_{2\perp}^2 \sim k_\perp^2 \sim \mathcal{M}^2(1-x)$. Hence their transverse velocities are $v_\perp \sim k_\perp/(1-x)p$, and in the lifetime $\tau \sim xp/\mathcal{M}^2$ of the large-mass virtual pair they can reach transverse distances of order

$$\Delta x_\perp \sim v_\perp \cdot \tau \sim \frac{k_\perp}{(1-x)\mathcal{M}^2} \sim \frac{1}{k_\perp}. \tag{3.3}$$

For low values of $k_\perp^2$, *i.e.* of the fixed scale $\mathcal{M}^2(1-x)$ of the interaction, the initially small virtual state can expand to typical hadronic size. Its scattering cross section is then large,[14]

$$\Delta x_\perp^2 \propto \frac{1}{\mathcal{M}^2(1-x)}. \tag{3.4}$$

It should be emphasized that even though the transverse size (3.4) of the virtual pair Fock state can be large, the overall production cross section of the massive pair at high x is still quite small, due to the low probability of finding the required Fock state in the projectile. However, when such Fock states scatter on nuclei, their large size will cause the reaction to be surface dominated, leading to an A^α

nuclear number dependence with $\alpha < 1$. Because the probability of the Fock state is linked to the projectile wavefunction, the suppression will show Feynman scaling, *i.e.* $\alpha = \alpha(x)$, as observed in the J/ψ production data.[1-3]

3.2 Fock State Probabilities

Let us now study the significance of the intrinsic diagrams more quantitatively. To keep the calculation as simple as possible, we shall consider bound states of scalar quarks and antiquarks in an abelian gauge theory. This avoids spin complications and also greatly decreases the number of diagrams that need to be considered. As may be readily verified for scalar QED in Coulomb gauge, instantaneous exchange dominates transverse photon exchange by a factor $1 - x$ in the large x limit.

We first calculate the probability of Fock states which contain an extra $q\bar{q}$ pair with invariant mass $\mathcal{M}$ and momentum fraction x. We will be interested in the combined limit (1.2). We will write the amplitude for the massive pair Fock state in the form

$$\Psi(\mu; u_1, u_2, \rho, \tau) = \frac{4\pi\alpha^2}{m^4}(1-x)^2 \int_0^1 dy \frac{\phi(yp, \vec{r}_\perp = \vec{0})}{[y(1-y)]^2} \frac{\tau(1-\tau)u_1u_2}{\mu\tau(1-\tau)u_1u_2 + u_1\tau + u_2(1-\tau)} F \tag{3.5}$$

where the last factor $F = F(\mu; u_1, u_2, \rho, \tau; y)$ of the integrand depends on the contributing diagram. Here m is the effective mass of the quarks while y, ρ and τ refer to their fractional momenta as indicated in Fig. 6. The integral over the transverse momentum in the bound state has been done, giving (as explained above) the bound state wavefunction ϕ evaluated at a vanishing transverse separation

$r_\perp = \mathcal{O}(1/\mathcal{M}) \sim 0$ between its constituents. The final state transverse momenta $p_{1\perp}$, $p_{2\perp}$ of the constituents are parameterized by

$$u_i = m^2/(m^2 + p_{i\perp}^2) \quad (i = 1, 2). \tag{3.6}$$

All dependence on the pair mass $\mathcal{M}$ will appear through the dimensionless parameter $\mu = (1-x)\mathcal{M}^2/m^2$, which is held fixed in the limit (1.2) under consideration. The explicit factor $(1-x)^2$ in Eq. (3.5) arises from the scaling of the two energy denominators involving the stopped quarks. The total probability to find a Fock state with pair mass $\mathcal{M}$ and pair momentum fraction x in the bound state is obtained by squaring the perturbative amplitude Ψ in (3.5) and integrating over the remaining variables,

$$\frac{d\mathcal{P}}{dx d\mathcal{M}^2} = \frac{m^4}{4p^2(4\pi)^6} \frac{1}{(1-x)} \int_0^1 d\tau d\rho du_1 du_2 \frac{|\Psi|^2}{u_1^2 u_2^2 \tau(1-\tau)}. \tag{3.7}$$

There are two extrinsic diagrams that give leading order contributions, the one shown in Fig. 6a and an analogous diagram where the pair is radiated off the other constituent. The sum of the two extrinsic diagrams give for the factor F in (3.5)

$$F_{\text{extrinsic}} = y(1+y)(1-2\rho)[u_2(1-\tau) - u_1\tau] \,, \tag{3.8}$$

where we have used the symmetry

$$\phi(yp, \vec{0}) = \phi((1-y)p, \vec{0}) \tag{3.9}$$

of the non-perturbative distribution amplitude.

If only extrinsic diagrams contribute, as would be the case for lepton pair production, we may now find the Fock state probability directly from Eqs. (3.8), (3.5) and (3.7). For quark pairs we have to add contributions from intrinsic diagrams, in which the pair is coupled to two or more gluons. An example of such a diagram, for our simple model, is shown in Fig. 6b. There are three other intrinsic diagrams, related by an opposite time ordering of the instantaneous exchanges and by a reverse ordering of the pair. The total intrinsic contribution to the factor F in Eq. (3.5) in the limit (1.2) is

$$F_{\rm intrinsic} = (2\rho - y)(1 + y - 2\rho)$$
$$\times \left\{ \theta(y-\rho) \left[\frac{\tau u_1}{\mu\tau u_1 y(1-\rho) + y - \rho} + \frac{(1-\tau)u_2}{\mu(1-\tau)u_2 y(1-\rho) + y - \rho} \right] \right.$$
$$\left. + \theta(\rho - y) \left[\frac{\tau u_1}{\mu\tau u_1(1-y)\rho + \rho - y} + \frac{(1-\tau)u_2}{\mu(1-\tau)u_2(1-y)\rho + \rho - y} \right] \right\} . \tag{3.10}$$

Notice that in contrast to the extrinsic contribution (3.8), the dependence of the Fock state amplitude (3.5) on the nonperturbative wavefunction ϕ does not factorize as a simple moment when F is given by (3.10), due to the more complicated dependence on y.

Since the factor F in (3.5) does not depend on x for fixed μ, the extrinsic and intrinsic diagrams of Fig. 6 give contributions to the perturbative wavefunction for pair production which have the same power behavior in $1-x$ in the limit (1.2). When the parameter μ becomes large, *i.e.* $\mathcal{M}^2 \gg m^2/(1-x)$, the extrinsic diagrams dominate due to the factor μ in the denominators of (3.10). On the other hand, for $\mu = \mathcal{O}(1)$ we see that $F_{\rm intrinsic}$ is larger than $F_{\rm extrinsic}$ near $y = \rho$. In this configuration the longitudinal momentum of each of the original constituents is close to that of a member of the pair.

A more quantitative estimate of the relative importance of the intrinsic diagrams requires a model for the nonperturbative distribution $\phi(yp, \vec{0})$. This amplitude should vanish rapidly at the end-points $y = 0$ and 1, since a configuration with either fermion having vanishing momentum would be far off its energy shell. Here we shall use

$$\phi(yp, \vec{0}) = c\, m\, p\, [y(1-y)]^2. \tag{3.11}$$

where the normalization is given by the dimensionless constant c. We have numerically evaluated the Fock state probability (3.7), both in the case when the amplitude (3.5) is given by the sum of all (six) extrinsic and intrinsic diagrams, and in the case when only the two extrinsic diagrams contribute. The former case would correspond to a quark pair structure function in QCD, while the latter represents lepton pair production. These probabilities could in principle be measured in deep inelastic scattering off the bound state. Figure 7 shows the ratio of the probabilities as a function of the parameter $\mu = (1-x)\mathcal{M}^2/m^2$. We note that the intrinsic diagrams dominate the extrinsic contributions for $\mu \lesssim 5$.

3.3 Pair Production Cross Sections

As a second example of physics in the limit (1.2), we will consider the cross section for large mass quark pair production in the peripheral scattering of a bound state off a heavy target. This process requires the materialization of the massive pair Fock state in the bound state wavefunction. At high energies, only a small momentum transfer ℓ to the target is required to put the pair on its energy shell. The momentum distribution of the produced pair will then be largely determined by its Fock state amplitude (3.5). Using the scalar quark theory of Subsection 3.2,

we will evaluate the scattering amplitude in the limit

$$p \gg \mathcal{M} \sim \frac{m_{i\perp}}{\sqrt{1-x}} \gg m_{i\perp} \gg \ell_\perp \,. \tag{3.12}$$

where $m_{i\perp}^2 = m^2 + p_{i\perp}^2$ (i=1,2) is the effective mass of the constituent valence quarks in the final state. As before, $\mu = (1-x)\mathcal{M}^2/m^2$ is held fixed.

A typical extrinsic diagram contributing to the peripheral scattering amplitude is shown in Fig. 8a. There are eleven other extrinsic diagrams analogous to Fig. 8a which contribute at leading order, differing by the time ordering of the instantaneous exchanges, by the scattering occurring off either constituent, and by the pair being emitted from either constituent. Diagrams with transverse exchanges or with scattering off the produced pair itself give non-leading contributions in the limit (3.12). It is convenient to write the scattering amplitude in the form

$$A = e^6 \frac{m_t}{\pi m^6 \ell_\perp^2}(1-x)^2 \int_0^1 dy \frac{\phi(yp, \vec{r}_\perp = \vec{0})}{[y(1-y)]^2} \left[\frac{\tau(1-\tau)u_1u_2}{\mu\tau(1-\tau)u_1u_2 + u_1\tau + u_2(1-\tau)}\right]^2 G \tag{3.13}$$

where m_t is the target mass. We find that the twelve extrinsic diagrams give the following contribution to the factor G in the integrand:

$$\begin{aligned} G_{\text{extrinsic}} = y(1+y)(2\rho-1)\Bigg\{ & \vec{\ell}_\perp \cdot \vec{p}_{1\perp} \frac{1-\tau}{\tau} u_2 \left[\frac{1}{\mu(1-\tau)u_2 + 1} + 1\right] \\ & + \vec{\ell}_\perp \cdot \vec{p}_{2\perp} \frac{\tau}{1-\tau} u_1 \left[\frac{1}{\mu\tau u_1 + 1} + 1\right]\Bigg\}, \end{aligned} \tag{3.14}$$

where $\vec{p}_{i\perp}$ ($i = 1,2$) are the transverse momenta of the original constituents in the final state, with magnitudes given by (3.6). Because the bound state is neutral, the numerator in (3.14) is of $\mathcal{O}(\ell_\perp)$. A similarity to the Fock state amplitude (3.8) may be seen. The scattering amplitude is, however, enhanced when the interacting constituent carries high transverse and low longitudinal momentum.

An example of an intrinsic diagram contributing at leading order to the scattering amplitude is shown in Fig. 8b. There are two other time orderings for the scattering of gluon ℓ on the lower constituent. Counting also the interactions of gluon ℓ on the upper constituent, we have altogether six diagrams that have a configuration of the produced pair as in Fig. 8b. Three other groups of six diagrams are obtained by interchanging the times of the instantaneous exchanges j_1 and j_2 attached to the pair, and by interchanging the momenta ($\rho \to 1-\rho$) of the pair. Hence there are 24 intrinsic diagrams in all that give a leading order contribution in the limit (3.12). As is the case for the extrinsic amplitude, diagrams with transverse exchanges or with scattering off the produced pair give non-leading contributions to the amplitude. Using the $y \to 1-y$ symmetry (3.9) of the distribution amplitude, the total intrinsic contribution to the factor G in (3.13) is

$$
\begin{aligned}
G_{\text{intrinsic}} &= (2\rho - y)(2\rho - y - 1) \\
&\times \left\{ \vec{\ell}_\perp \cdot \vec{p}_{1\perp} \frac{1-\tau}{\tau} u_2 \left[\frac{1}{\mu y(1-\rho)(1-\tau)u_2 + y - \rho} + \frac{1}{\mu(1-y)\rho(1-\tau)u_2 + \rho - y} \right] \right. \\
&\left. - \vec{\ell}_\perp \cdot \vec{p}_{2\perp} \frac{\tau}{1-\tau} u_1 \left[\frac{1}{\mu y(1-\rho)\tau u_1 + y - \rho} + \frac{1}{\mu(1-y)\rho\tau u_1 + \rho - y} \right] \right\} .
\end{aligned}
\tag{3.15}
$$

Notice that the denominators in (3.15) can vanish inside the integration region, and therefore have to be regulated with the $+i\epsilon$ prescription. Hence the intrinsic production amplitude is complex.[15] The physical reason for this can be understood by considering the intermediate state indicated by the cut in the diagram of Fig. 8b. The energy difference (3.1) of this state is, to leading order in the limit (3.12),

$$
\Delta E(8b) = \frac{m^2}{2p(1-x)\tau u_1} \left[1 - \frac{\mu y(1-\rho)\tau u_1}{\rho - y} \right] . \tag{3.16}
$$

Since $\rho - y > 0$ in this diagram, the energy difference will change sign in the interval $0 < y < \rho$. When (3.16) vanishes a threshold is crossed for real pair production in the intermediate state. Loosely speaking, the extra energy required to stop constituent 1 is compensated by the energy gained from having accelerated the particle in the pair, which has a large effective mass of $\mathcal{O}(\mathcal{M})$. As we shall discuss in Section 4, the fact that the intrinsic amplitude is complex in leading order can give rise to transverse polarization effects in the real world with spin $\frac{1}{2}$ quarks.

It is also interesting to observe that the intrinsic amplitude (3.15) vanishes not only for large μ, but also as $\mu \to 0$, which corresponds to the limit (1.3). Hence only extrinsic contributions are relevant in calculating the $x \to 1$ end-point behavior of the cross section. The physical reason for this is that in intrinsic processes the quark pair is created at transverse distances $r_\perp \sim \sqrt{1-x}/m_h$, which for small μ are shorter than the Compton wavelength $1/\mathcal{M}$ of the pair. This mismatch is avoided in extrinsic processes.

The pair production cross section is given in terms of the amplitude (3.13) by

$$\frac{d\sigma}{dx d\mathcal{M}^2 d^2\vec{\ell}_\perp} = \frac{4}{(4\pi)^{10}} \frac{1}{m_i^2 p^2} \frac{1}{1-x} \int_0^\infty d^2p_{1\perp}\, d^2p_{2\perp} \int_0^1 \frac{d\rho d\tau}{\tau(1-\tau)} |A|^2. \qquad (3.17)$$

We have evaluated the cross section numerically using the model wavefunction (3.11) for the bound state. In Fig. 9 we show the ratio of the cross section calculated using $A = A_{\rm extrinsic} + A_{\rm intrinsic}$ to that obtained with $A = A_{extrinsic}$ as a function of the parameter μ. As expected, the ratio approaches unity in both the large and small μ limits where the intrinsic diagrams vanish. However, for intermediate values of μ the intrinsic diagrams are important. Somewhat unexpectedly, the intrinsic contribution remains sizeable up to quite large values of μ.

This might imply that there can be important intrinsic effects in realistic heavy quark processes even at only moderately large values of x. The numerical values obtained in our simple model of course should only be taken as an indication of what might be expected in QCD.

4. Summary and Conclusions

As we have seen in this paper, there are a number of novel features of QCD which emerge when massive lepton or quark pairs are examined in the large x domain. We have particularly focussed on a new QCD limit (1.2) where the pair mass $\mathcal{M}^2$ is large but $(1-x)\mathcal{M}^2$ is fixed. In this new QCD limit:

- The leading contributions to the production cross section actually come from spectator interactions rather than direct interactions with the pair itself;
- The coherence of the Fock state is easily broken by soft interactions of finite transverse momentum since the transverse velocity inflicted to the spectators $v_\perp = p_\perp/p(1-x)$ is large;
- QCD factorization is invalid in this limit since there is no relative suppression of interactions involving several constituents of the same hadron;
- The nuclear target dependence of the production cross section in this limit is a function $A^{\alpha(x)}$ of the pair momentum fraction x rather than a function $A^{\alpha(x_2)}$ of the target parton momentum fraction x_2;
- Because of the rapid transverse size expansion of the spectators, production cross sections in nuclear targets become surface dominated at large x;
- The intrinsic mechanism offers the possibility to produce the J/ψ directly in a color singlet state. In analogy to Fig. 6b, the three quarks of a proton may

all couple to the J/ψ via gluon exchange. Hence there is no need for further soft gluon radiation;[16]

- Although the absolute normalization of the intrinsic contributions to massive pair production requires knowledge of two or more particle correlations in the non-perturbative hadron wavefunction, it is still possible to use QCD perturbation theory to analyze both the power law behavior and logarithmic evolution of these contributions in a manner analogous to PQCD treatments of large momentum transfer exclusive reactions,[10] since the short-distance components of the wavefunction dominate. In particular, the extrapolation from charm to beauty processes is straightforward using scaling at fixed $\mu = \mathcal{M}^2(1-x)$.

Our investigation can provide a QCD framework for understanding a number of puzzling features of the large x data:

- The nuclear suppression seen for J/ψ production is much larger than that for $\mu^+\mu^-$ production.[3] Only extrinsic diagrams of the type shown in Fig. 5b contribute to the lepton pair process, whereas also intrinsic contributions like Fig. 5c exist for quark pairs. In a simple model we found that for intermediate values of $\mathcal{M}^2(1-x)$ the intrinsic diagrams can dominate the production cross section. If this interpretation of the data is correct, it suggests very important intrinsic contributions to J/ψ production in QCD.
- Another consequence of large intrinsic contributions is that the charm and beauty structure functions measured in deep inelastic scattering can have a larger than expected support at high x_{Bj}. There is some evidence for this from EMC measurements of the charm structure function of the nucleon.[17] This will be an important area of investigation at HERA.

- The intrinsic reaction mechanism that we have studied may give an explanation of the surprisingly large rates of open and hidden charm production observed* at high x, as well as of the leading particle effect. Previous models have postulated a 'recombination',[19] or 'string acceleration',[20] of slow heavy quarks by fast valence quarks, to boost the fast charm rate. However, such a mechanism could not correspond to a soft process, since the momentum exchange between the light and heavy quarks is required to be large. Hence the acceleration process should be treated using PQCD. In the intrinsic diagram of Fig. 8b we see an example of this, where a heavy quark produced off one constituent later absorbs momentum from the other. After the heavy quark has gained momentum, it can coalesce with co-moving light quarks at low x through a soft process. This gives an immediate interpretation for the existence of leading particle effects in open charm and beauty production.* Coalescence is enhanced in gauge theories when the quarks have the same velocity or rapidity. A QED analog is explored in Ref. 23. Unlike recombination and string pictures, where fast valence quarks pull the heavy particles to high momenta, the intrinsic heavy quark picture implies not only fast open charm and beauty states, but also heavy quarkonium production at large x.
- The intrinsic production mechanism offers an intriguing new possibility of understanding 'cumulative' meson production in nuclei at large transverse

---

* Note that the dashed curve shown in Fig. 11a of Ref. 18, which already is below the data, is the prediction of extrinsic QCD assuming that the D meson carries all of the momentum of the charm quark. In fact it is known from e^+e^- data that the meson on average only carries 70% of the quark momentum. Hence the QCD prediction should be correspondingly reduced.

* This same effect can also account for the observed suppression of quarkonium production in the nuclear fragmentation region in E772[3] and at high particle density in heavy ion collisions in NA38.[21] For a recent discussion and references see Ref. 22.

momentum.[24,25] As has been established in many experiments, a particle produced in the nuclear fragmentation region can carry more momentum than single nucleons ($x > 1$). The two (or more) gluons transferring momentum to the heavy quarks in intrinsic processes, such as the one in Fig. 6b, need not, in fact, originate from the same nucleon. Two or more nucleons with a small transverse separation can both transfer momentum to the same quark pair. Moreover, the number of intrinsic diagrams increases quickly with the nuclear number A and the number of gluons involved.

- Among the puzzles of particle production at high x is the observed dependence on the transverse polarization of the beam. Recent data[26] show a remarkable increase of the polarization asymmetry in the region $0.3 < x < 0.9$. It has been difficult to describe such polarization effects in the framework of perturbative QCD because the polarization is given by an interference term between flip and non-flip amplitudes,

$$P\frac{d\sigma}{dt} \sim Im(A_f^* A_{nf}). \tag{4.1}$$

In leading twist QCD calculations very small transverse polarizations are expected, since the helicity flip amplitudes are suppressed and the amplitudes are predominantly real.[27] On the other hand, as we noted in Section 3.3, the intrinsic diagrams such as Fig. 8b have a sizeable imaginary part, which appears immediately in the lowest order amplitude. Furthermore, the incoming Fock state involves large transverse momenta for the constituents, which can lead to important helicity flip contributions. It would thus appear that, assuming helicity flip amplitudes are prsent, the intrinsic production mechanism may be a dominant source of transverse polarization effects. This is

supported by the fact that the observed polarization increases with the transverse momentum of the detected hadron. It is in the combined limit of large x and high pair mass (*i.e.* high $p_\perp$) that the intrinsic diagrams contribute at leading order.

- One of the most striking consequences of the analysis of this paper is the prediction for the soft, low $Q^2 \sim \mathcal{M}^2(1-x)$, Coulomb excitation of the proton to high x massive quark pair configurations, especially $ep \to e' + J/\psi + X$ and other heavy quarkonium states. The dominant diagrams at $x \to 1$ involve the electron scattering on the valence spectators, not on the heavy quarks themselves. The absolute size of the cross section can be estimated from J/ψ production in proton–proton collisions, assuming factorization. A critical test of the importance of higher twist correlations in the proton wavefunction will be the observation of quarkonium states at large x in the proton's fragmentation region. Furthermore, if intrinsic diagrams such as Fig. 8b account for the transverse polarization observed in high x hadronic reactions, then similar polarization effects should be present in peripheral ep collisions. It will be important to test these predictions at HERA.

Acknowledgements

P. H. wishes to thank the SLAC theory group for its warm hospitality during his sabbatical. S. J. B. and A. H. M. also wish to thank the Department of Theoretical Physics at Lund for their hospitality.

Appendix

In calculating hadron scattering amplitudes mediated by gluon exchange, it is convenient to view the hadron as a source for gluon pairs, as shown in Fig. 10. We may define the source amplitude as

$$\mathcal{S}^{ab}_{\mu\nu}(\ell) = (2\pi)^3 2E_p \; Im \int \frac{d\ell^+}{2\pi} \int d^4y \, \exp(-i\ell\cdot y) \, \langle P| \, A^b_\nu(0) \, A^a_\mu(y) \, |P\rangle \qquad (4.2)$$

where A^a_μ is the gluon field and $|P\rangle$ is a hadron of momentum P. The connection to the usual leading logarithmic gluon distribution is

$$xG(x,Q^2) = \sum_a \int \frac{d^2\vec{\ell}_\perp d\ell^-}{(2\pi)^3} \, \mathcal{S}^{aa}_{\mu\nu}(\ell) \, P^{\mu\nu}(\ell) x^2 \delta\left(x - \frac{\ell^-}{P^-}\right) \Theta(Q^2 - \ell^2_\perp) \qquad (4.3)$$

where

$$P_{\mu\nu}(\ell) = -\left(g_{\mu\nu} - \frac{\overline{\eta}_\mu \ell_\nu + \overline{\eta}_\nu \ell_\mu}{\overline{\eta}\cdot\ell} + \ell^2 \frac{\overline{\eta}_\mu \overline{\eta}_\nu}{(\overline{\eta}\cdot\ell)^2}\right) \qquad (4.4)$$

with $\overline{\eta}\cdot v = v^-$ for any vector v. We may write

$$\mathcal{S}^{ab}_{\mu\nu}(\ell) = 2P^- \, \delta_{ab} \, \mathcal{S}(\vec{\ell}_\perp, x) \, \frac{\ell^\perp_\mu \ell^\perp_\nu}{(\ell^2_\perp)^2 \ell^{-2}} \qquad (4.5)$$

in light-cone gauge and

$$\mathcal{S}^{ab}_{\mu\nu}(\ell) = 2P^- \, \delta_{ab} \, \mathcal{S}(\vec{\ell}_\perp, x) \, \frac{\eta_\mu \eta_\nu}{(\ell^2_\perp)^2} \qquad (4.6)$$

in covariant gauge, with $\eta\cdot v = v^+$. Eqs. (4.5) and (4.6) are correct in the small x, high energy, limit.

REFERENCES

1. J. Badier *et al.*, Z. Phys. C20 (1983) 101.

2. S. Katsanevas *et al.*, Phys. Rev. Lett. 60 (1988) 2121.

3. D. M. Alde *et al.*, Phys. Rev. Lett. 66, 2285 (1991); 66, 133 (1991); 64, 2479 (1990), and C. S. Mishra, *et al.*, Contribution to the XXVth Rencontres de Moriond, Les Arcs (1990), Fermilab–Conf–90/100–E (May 1990).

4. P. Hoyer, M. Vänttinen and U. Sukhatme, Phys. Lett. 246B, 217 (1990). See also Ref. 3.

5. S. J. Brodsky and P. Hoyer, Phys. Rev. Lett. 63 (1989) 1566. [A different proposal is given in G. Bertsch, S. J. Brodsky, A. S. Goldhaber and J. Gunion, Phys. Rev. Lett. 47, 297 (1981).] A phenomenological analysis is given in R. Vogt, S. J. Brodsky and P. Hoyer, SLAC-PUB-5421 (1991).

6. S. J. Brodsky, P. Hoyer, C. Peterson, and N. Sakai, Phys. Lett. 93B, 451 (1980); S. J. Brodsky, C. Peterson, and N. Sakai, Phys. Rev. D23, 2745 (1981).

7. S. J. Brodsky, J. C. Collins, S. D. Ellis, J. F. Gunion and A. H. Mueller, in *Proceedings of the Summer Study on the Design and Utilization of the Superconducting Super Collider,* Snowmass, CO, 1984, edited by R. Donaldson and J. Morfin (Division of Particles and Fields of the American Physical Society, New York, 1985).

8. J. C. Collins, D. E. Soper and G. Sterman, published in *Perturbative QCD*, edited by A.H. Mueller, World Scientific, (1989); G. Bodwin, Phys. Rev. D31 2616, (1985), D34 3932, (1986E); Jian-wei Qiu and G. Sterman, Nucl. Phys. B353 105, 137 (1991). Leading twist perturbative QCD calculations

for heavy quark production are given in P. Nason, S. Dawson, and R.K. Ellis, Nucl. Phys. B327 49 (1989); and in W. Beenakker, W. L. van Neerven, R. Meng, G.A. Schuler and J. Smith, Stony Brook preprint ITP-SB-90-46, (1990).

9. R. Blankenbecler and S. J. Brodsky, Phys. Rev. D10, 2973 (1974); J. Gunion, Phys. Rev. D10, 242 (1974). A review is given in D. Sivers, S. J. Brodsky and R. Blankenbecler, Phys. Reports 23C, 1 (1976).
10. For a review and further references see S. J. Brodsky and G. P. Lepage, published in *Perturbative Quantum Chromodynamics*, Edited by A. H. Mueller, World Scientific (1989).
11. A related phenomenon has been predicted for lepton pair production in meson-nucleon collisions where a higher twist C/Q^2 contribution involving the meson wave function dominates the leading twist $(1-x)^2$ contribution from the meson structure function at large x. See E. L. Berger and S. J. Brodsky, Phys. Rev. Lett. 42, 940 (1979).
12. When spin is taken into account, there is an additional term in the exponent equal to twice the helicity flip. See Z. F. Ezawa, Nuovo Cim. 23A, 271 (1974); G. P. Lepage and S. J. Brodsky, Phys. Rev. D22, 2157 (1980); S. Brodsky, J. Gunion and M. Scadron (unpublished).
13. A physical gauge is assumed in Fig. 5b.
14. Since the initial valence quark state has a small size it interacts weakly due to color transparency. See S. J. Brodsky and A. H. Mueller, Phys. Lett. 206B, 685 (1988), and references therein. However, the rapid expansion of the Fock state after the heavy pair is produced at large x effectively leads to 'color opacity.'

15. For a useful physical discussion of this type of imaginary parts, see A. S. Kronfeld and B. Nizic, Fermilab-Pub-91-64-T (1991).

16. For a related proposal, see J. Milana, Phys. Rev. Lett. 62, 2921 (1989).

17. J. J. Aubert, *et al.*, Nucl. Phys. B213, 31 (1983). For a recent discussion and further references, see C. S. Kim, Nucl. Phys. B353, 87 (1991). See also E. Hoffmann and R. Moore, Z. Phys. C20, 71 (1983).

18. M. Aguilar-Benitez, *et al.*, Z.Phys. C40, 321 (1988).

19. R. C. Hwa and M. S. Zahir, Z. Phys. C20, 27 (1983) and references therein.

20. H. U. Bengtsson and G. Ingelman, Comp. Phys. Commun. 34, 231 (1985).

21. C. Baglin, *et al.*, Can. J. Phys. 67, 1222 (1989).

22. R. Vogt, S. J. Brodsky and P. Hoyer, SLAC-PUB-5421 (1991).

23. S. J. Brodsky, J. F. Gunion and D. E. Soper, Phys. Rev. D36, 2710 (1987).

24. P. Hoyer and S. J. Brodsky, Proc. of the Topical Conference on Particle Production Near Threshold, Nashville, Indiana, (1990), AIP Conf. Proc. #221, pg. 238.

25. For a review on the cumulative effect and references see L. L. Frankfurt and M. I. Strikman, Phys. Rep. 160, 235 (1988).

26. D. L. Adams, *et al.*, Rice University preprint DOE/ER/05096-45 (1991), and references therein.

27. See also D. Sivers, Phys. Rev. D43, 261 (1991); D41, 83 (1990).

FIGURE CAPTIONS

1) A contribution to the forward elastic electron–electron amplitude, the imaginary part of which (indicated by the vertical cut) gives the cross section for $ee \to \mu^+\mu^-\, ee$ through the subprocess $\gamma\gamma \to \mu^+\mu^-$.

2) Forward amplitudes for $ee \to ee$, whose absorptive parts give contributions to the $ee \to \mu^+\mu^-\, ee$ cross section through the $\gamma + e \to \mu^+\mu^- + e$ subprocess.

3) The analog of Fig. 2 in the case of hadron–hadron scattering.

4) A perturbative contribution to the proton wavefunction, in which one quark carries most of the momentum xp, with $x \to 1$. The momentum $(\vec{k}_\perp, yp)$ carried by the same quark in the non-perturbative wavefunction is integrated over.

5) Amplitudes for quark or lepton pair production in a peripheral collision of a meson with momentum p. The invariant mass of the pair is $\mathcal{M}$, and its 3-momentum $(\vec{k}_\perp, xp)$. (a) A leading twist diagram, which does not involve the spectator quark. (b) A non-leading twist extrinsic diagram, where the pair is radiated from only one constituent. (c) A non-leading twist intrinsic diagram, in which the produced pair is connected to both constituents. The curved vertical line indicates the absorptive part.

6) Perturbative contributions to a meson Fock state with an extra quark pair of large mass $\mathcal{M}$ and high longitudinal momentum xp ($x \to 1$). The fractional momenta of the particles are indicated. Dashed lines indicate instantaneous Coulomb exchanges. (a) An extrinsic diagram. (b) An intrinsic diagram.

7) Ratio of the Fock state probability (3.7) calculated using both extrinsic and intrinsic diagrams to that calculated with only the extrinsic diagrams, as a

function of $\mu = \mathcal{M}^2(1-x)/m^2$.

8) Production amplitudes for a quark pair of mass $\mathcal{M}$ and longitudinal momentum xp, in a peripheral Coulomb scattering of a meson from an elementary target of mass m_t. The curved vertical line indicates an absorptive part.

9) Ratio of the pair production cross section (3.17) calculated using both the extrinsic and intrinsic diagrams to that calculated with only the extrinsic diagrams, as a function of $\mu = \mathcal{M}^2(1-x)/m^2$.

10) Pictorial representation of the gluon source $\mathcal{S}^{ab}_{\mu\nu}(\ell)$ of Eq. (4.2), viewed as the absorptive part of a forward gluon–hadron amplitude.

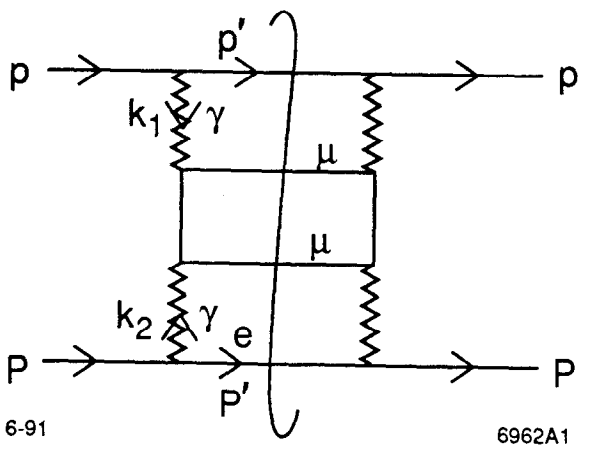

Fig. 1

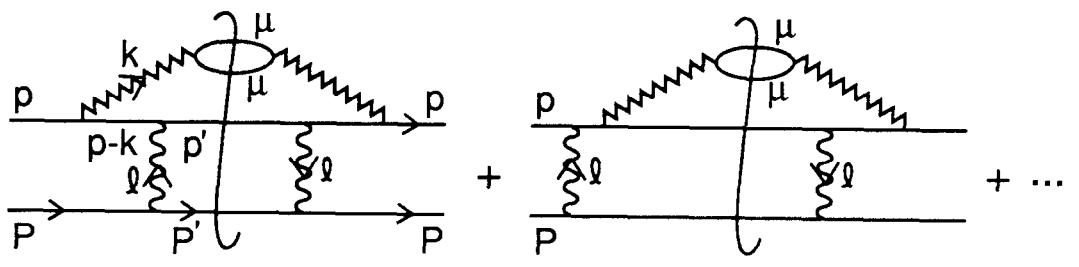

6-91

6962A02

Fig. 2

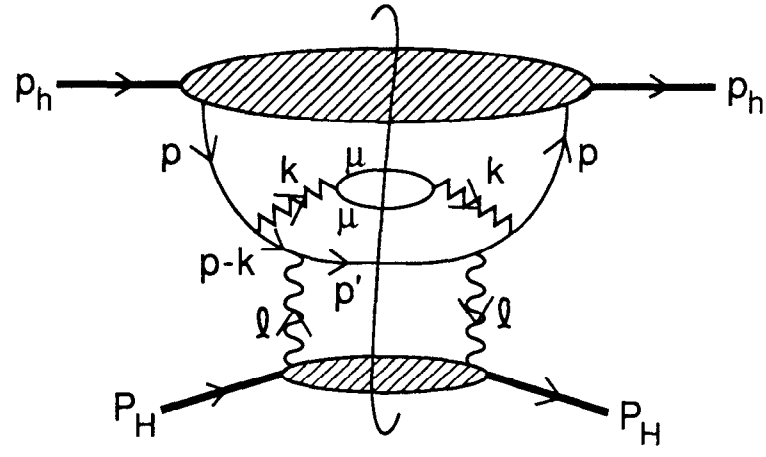

6-91

6962A3

Fig. 3

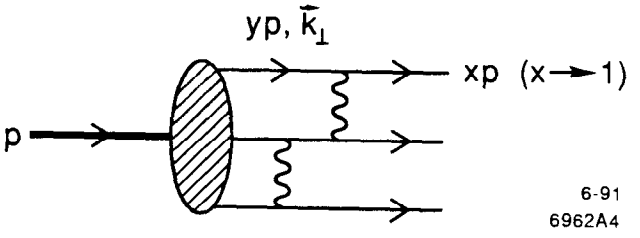

Fig. 4

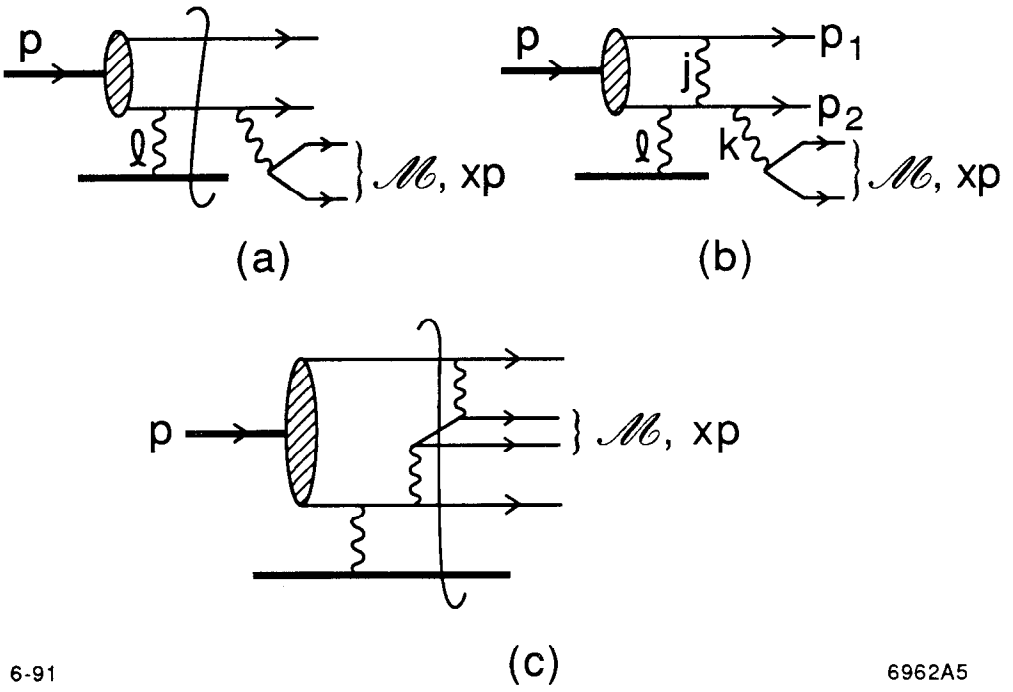

Fig. 5

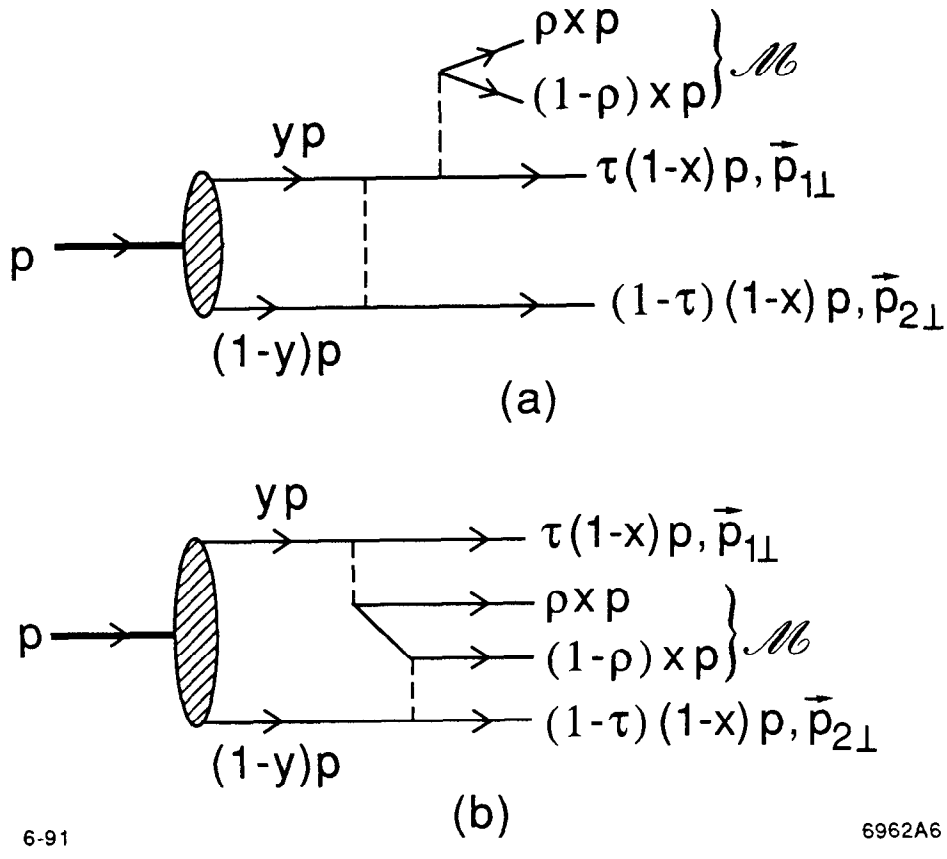
ρxp
(1-ρ)xp
ℳ
yp
τ(1-x)p, p̄1⊥
p
(1-τ)(1-x)p, p̄2⊥
(1-y)p
(a)
yp
τ(1-x)p, p̄1⊥
ρxp
(1-ρ)xp
ℳ
p
(1-τ)(1-x)p, p̄2⊥
(1-y)p
(b)
6-91
6962A6

Fig. 6

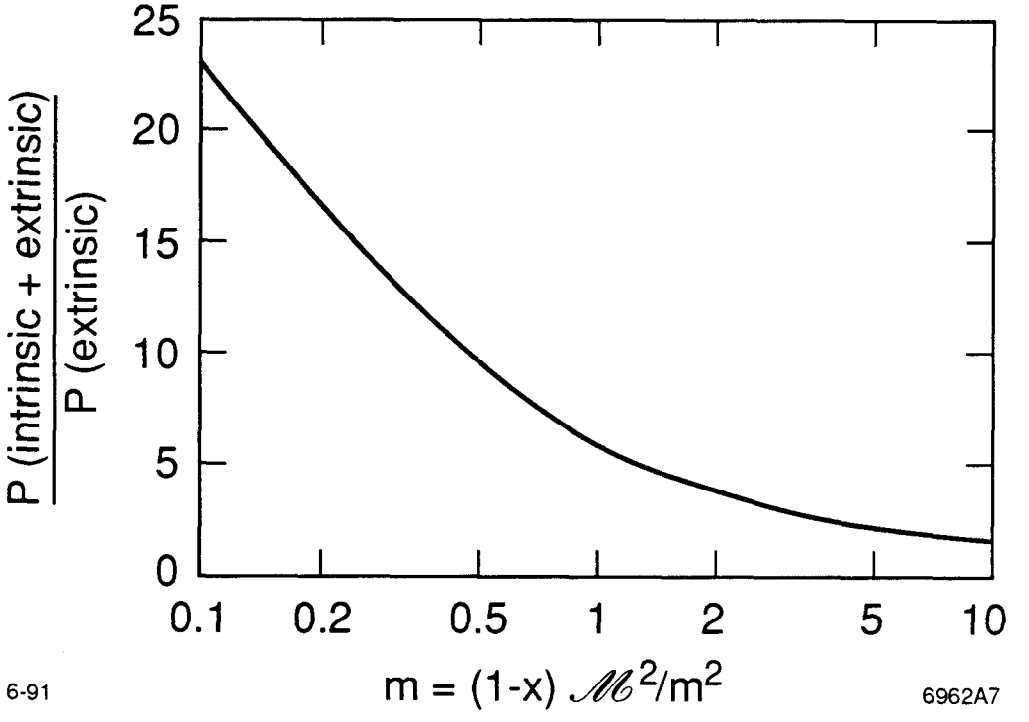
25
20
15
10
5
0
0.1
0.2
0.5
1
2
5
10
P (intrinsic + extrinsic) / P (extrinsic)
m = (1-x) $\mathscr{M}^2/m^2$
6-91
6962A7

Fig. 7

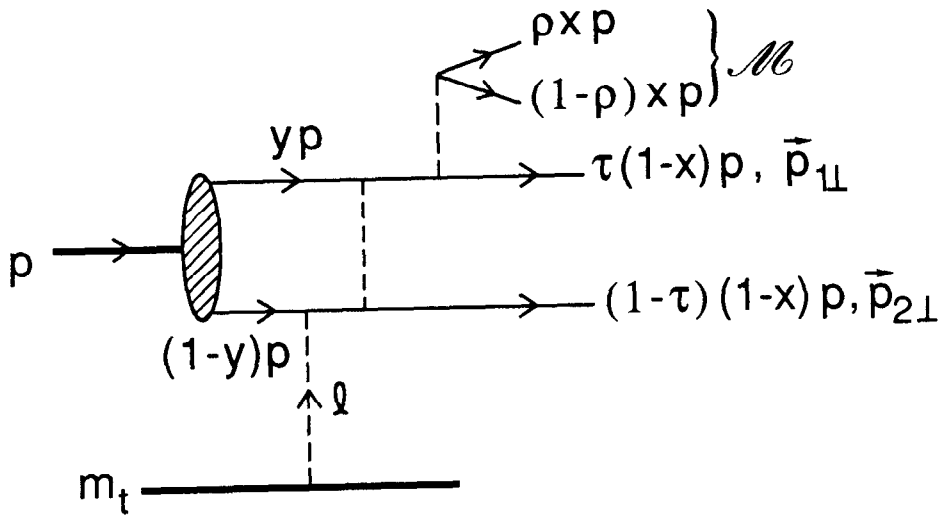

(a)

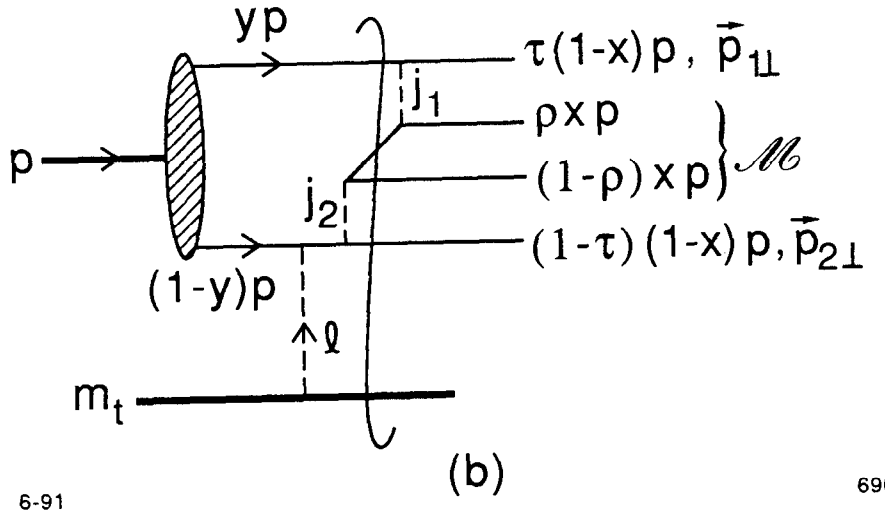

(b)

6-91

6962A8

Fig. 8

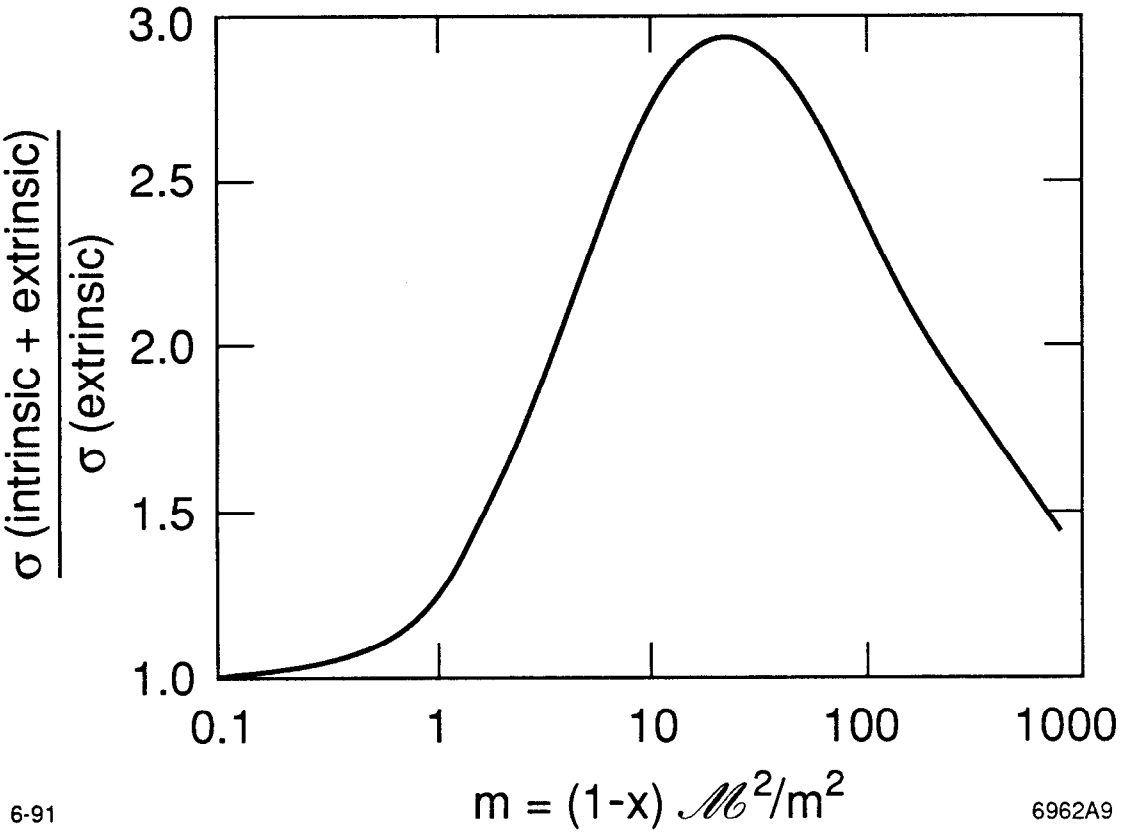
3.0
2.5
2.0
1.5
1.0
σ (intrinsic + extrinsic) / σ (extrinsic)
0.1
1
10
100
1000
m = (1-x) $\mathscr{M}^2/m^2$
6-91
6962A9

Fig. 9

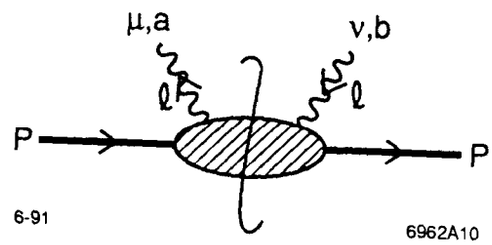

Fig. 10